Pharm Res (2015) 32:562–577
DOI 10.1007/s11095-014-1486-0

RESEARCH PAPER

Folate-Targeted Multifunctional Amino Acid-Chitosan Nanoparticles for Improved Cancer Therapy

Vítor M. Gaspar • Elisabete C. Costa • João A. Queiroz • Chantal Pichon • Fani Sousa • Ilídio J. Correia

Received: 21 May 2014 / Accepted: 15 August 2014 / Published online: 4 September 2014

ABSTRACT

Purpose Tumor targeting nanomaterials have potential for improving the efficiency of anti-tumoral therapeutics. However, the evaluation of their biological performance remains highly challenging. In this study we describe the synthesis of multifunctional nanoparticles decorated with folic acid-PEG and dual amino acid-modified chitosan (CM-PFA) complexed with DNA and their evaluation in organotypic 2D co-cultures of cancer-normal cells and also on 3D multicellular tumor spheroids models.

Methods The physicochemical characterization of CM-PFA multifunctional carriers was performed by FTIR, ^{1}H NMR and DLS. 2D co-culture models were established by using a 1:2 cancer-to-normal cell ratio. 3D organotypic tumor spheroids were assembled using micromolding technology for high throughput screening. Nanoparticle efficiency was evaluated by flow cytometry and confocal microscopy.

Results The CM-PFA nanocarriers (126–176 nm) showed hemocompatibility and were internalized by target cells, achieving a 3.7 fold increase in gene expression. *In vivo*-mimicking 2D co-cultures confirmed a real affinity towards cancer cells and a negligible uptake in normal cells. The targeted nanoparticles penetrated into 3D spheroids to a higher extent than non-targeted nanocarriers. Also, CM-PFA-mediated delivery of p53 tumor suppressor promoted a decrease in tumor-spheroids volume.

Conclusion These findings corroborate the improved efficiency of this delivery system and demonstrate its potential for application in cancer therapy.

Electronic supplementary material The online version of this article (doi:10.1007/s11095-014-1486-0) contains supplementary material, which is available to authorized users.

V. M. Gaspar • E. C. Costa • J. A. Queiroz • F. Sousa • I. J. Correia (✉)
CICS-UBI – Health Sciences Research Centre, Universidade da Beira Interior, Avenida Infante D. Henrique, 6200-506 Covilhã, Portugal
e-mail: icorreia@ubi.pt

C. Pichon
Centre de Biophysique Moléculaire, CNRS UPR4301, Inserm and University of Orléans, 45071 cedex 02 Orléans, France

KEY WORDS cancer therapy · gene delivery · targeted nanoparticles · 2D co-cultures · 3D tumor spheroids

INTRODUCTION

Targeted delivery through specialized nanocarriers currently attracts remarkable attention since bioactive molecules can be selectively transported into malignant tissues with improved efficiency and limited systemic toxicity (1). In line with this focus, nanosized systems are currently being developed for the delivery of a broad range of anti-tumoral therapeutics that span from plasmid DNA (pDNA (2)), small interfering RNA (siRNA (3)), polyphenolic compounds (Resveratrol, tea catechins (4)), up to general pharmaceuticals (Doxorubicin, Paclitaxel and Cisplatin (5)).

Nevertheless, despite these advances, the majority of the nanocarriers engineered so far present limited *in vivo* targeting capacity, generally taking advantage of a probabilistic accumulation in cancer cells through the so-termed enhanced permeability and retention effect (EPR) (6). The EPR effect is a consequence of an uncontrolled angiogenesis which originates disorganized and leaky vascular networks that have characteristic fenestrations with sufficiently large sizes for passive nanocarrier extravasation into diseased tissues (100 - 300 nm) (7,8). However, this range is highly variable, depends on tumor type, location, and vascular density, both at the periphery and tumor core (9). To further hinder accumulation, solid tumors have a high interstitial fluid pressure, an additional barrier that affects nanoparticle convective diffusion and tissue penetration (10). Consequently, these properties significantly impair the pharmacokinetic/pharmacodynamic profile and therapeutic effectiveness of non-targeted delivery systems (9,11). In order to overcome these issues various classes of targeting ligands such as antibodies (Herceptin®(12)), aptamer bioconjugates (13), homing

peptides (14), and other macromolecules including lectins (12), transferrin (Tf) (15), and folic acid (FA) (12), are available for cell targeting. In this context, selecting ligands that bind surface receptors prone to internalization is a valuable strategy to deliver drugs and DNA biopharmaceuticals that are only active in the cytoplasm or nucleus (2). For this objective, FA is a particularly advantageous biomolecule since it can bind to the folate receptor (FR) with high affinity under physiological conditions ($Kd \approx 1 \times 10^{-10}$ M), and is then readily internalized via receptor-mediated endocytosis (16,17). The fact that folate receptors have minimal expression in most tissues and are highly expressed in breast, cervical, ovary and prostate cancers (18,19), further contributes for their potential to be used as a target for cancer therapy (17,20). In a recent report, Aranda *et al.*, 2013, demonstrated that the use of folate-conjugated cyclodextrin derivatives significantly enhanced gene transfer into FR-positive cancer cells, with target-specific polyplexes achieving a 1.7 fold increased expression in comparison with plain nanocarriers (21). On the other hand, folate functionalization by itself has shown certain limitations in promoting penetration into deep tumor regions, a fact that presents a major issue in current nanomedicines under production. Such could be overcome, by combining FR targeting with cell penetrating moieties like the TAT penetrating protein (22). In the same way, our group has recently reported the formulation of amino acid modified nanoparticles that remarkably improve cell penetration through the use of arginine moieties and also stimulate endosomal release of pDNA carriers by the pH responsive behaviour of histidine, in an effort to improve the therapeutic outcome (23).

However, up until recently, testing the biological activity after nanocarrier modification with targeting ligands or penetration enhancers remained extremely challenging during pre-clinical stages (24). A fact mainly attributed to the lack of *in vitro* tools capable of providing data that can be correlated with the complex *in vivo* conditions (25). This necessity assumes additional importance in light of the current restrictions of animal use and also of the rigorous toxicity-efficiency tests demanded by regulatory organisms (FDA, EMEA) before nanomedicines clinical approval (26). In this stand point, the advent of 2D co-cultures and 3D solid tumor models presents a relevant breakthrough (27,28). Co-culture models have various advantages over standard single cell culture, in such a way that the targeting capacity of nanocarriers can be simultaneously tested in a heterogeneous culture of malignant and normal cells (25). These assays thus provide valuable insights in to true cell-selectivity. In addition, 3D multicellular tumor spheroids (MCTS) is another useful platform for testing the development of nanocarriers since these microtissues can closely mimic *in vitro* the complex tumor architecture, mass transfer limitations, cell-cell contacts, pH gradients and necrotic regions with high accuracy (26). Besides, by using novel nano/micro manufacturing technologies for MCTS production, a large number of uniform spheroids can be produced simultaneously, contributing for robust assays and data acquisition (29).

Therefore, herein we report the formulation of a multifunctional nanocarrier comprised by folate-PEG and amino acid moieties (CM-PFA) to improve cell targeting and penetration. The biological performance of this novel nanocarrier was evaluated in 2D co-cultures and 3D solid tumor models produced by micropatterned scaffolds. Altogether our results show that this delivery system has improved cell uptake, tumor penetration and also gene expression in 3D spheroids.

MATERIALS AND METHODS

Materials

Folic acid, branched Polyethylenimine (PEI) (Mw≈25 kDa), L-cysteine, L-histidine, L-arginine, Triethylamine (TEA), cysteamine. HCl, Fluorescein isothiocyanate isomer I (FITC), Rhodamine B isothiocianate (RITC), N- Hydroxysuccinimide (NHS), 4-(2-Hydroxyethyl)piperazine-1-ethanesulfonic acid (HEPES), Resazurin, cell culture Dulbecco's Modified Eagle's Medium – high glucose (DMEM-HG) and DMEM-F12 were purchased from Sigma–Aldrich (Sintra, Portugal). Fetal bovine serum (FBS) was acquired from Biochrom (Biochrom AG, Berlin). N-(3-Dimethylaminopropyl)-N'-ethylcarbodiimide hydrochloride (EDAC) was obtained from MerckMillipore (Nothingham, UK). Homobifunctional Poly(ethylene glycol) maleimide (MAL-PEG-MAL, MW≈3500 Da) was acquired from Nanocs Inc (New York, USA). Pharmaceutical-grade chitosan UP CL 113 (MW≈110 kDa; Deacetylation degree: 83%; Heavy metals <16 ppm, Proteins: 0.09%; Endotoxins <51 EU/gram) was purchased from Novamatrix (Sandvika, Norway). HeLa (Human negroid cervix epitheloid carcinoma - CCL-2) cells were acquired from ATCC (Middlesex, UK). Human dermal fibroblasts (hFIB) were obtained from Promocell (Heidelberg, Germany). The fluorescent probes Hoechst 33342® and Backman Cell Light 2.0® Actin-GFP, were obtained from Invitrogen (Carlsbad, CA, USA). Anti-F-actin CruzFluor® 647 conjugate antibody was a kind gift from Santa Cruz Biotechnology (Santa Cruz, CA, USA). All the buffers and reagents used were of technical or analytical grade.

Methods

A complete description of all the methods technical details is provided in supplementary information.

Synthesis of Folate- PEG-Amino Acid Modified Chitosan

The synthesis of amino acid-modified chitosan (CM) was performed through selective amidation of the polymer primary amines by using EDC/NHS coupling chemistry as previously reported by our group (23). The inclusion of PEG into CM polymer was promoted via thiol-maleimide Michael-type addition reaction. For the synthesis of folate-grafted polymers (CM-PFA) an excess of FA-SH was reacted with CM-P via Michael type thiol-maleimide coupling, as previously described by Zhang and co-workers, 2010 (30). To remove unreacted folic acid the product was initially dialyzed (MWCO 3500 Da) against 5 L of 0.1 M sodium bicarbonate solution during 4 days, in the dark. The use of sodium carbonate leads to the formation of sodium folate, i.e., the soluble salt of folic acid allowing its removal. Afterwards, the product was dialyzed against 5 L of water for additional 4 days in the dark. The recovered product was then freeze dried for 48 h, and stored at 4°C until further use, in the dark, to protect folic acid from degradation (yield, 81.9%). Characterization of CM-PFA multifunctional polymers was performed through ^{1}H NMR spectroscopy and Fourier transform infrared spectroscopy (FTIR) (Fig. S1, S2, S3 and S4).

Formulation of Targeted Multifunctional Nanocarriers

For the formulation of CM-PFA/pDNA polyplexes a stock solution of modified polymers was prepared in 5 mM sodium acetate (NaAct) buffer (pH 4.5). The CM-PFA/pDNA polyplexes were assembled at different molar ratios of polymer amines to pDNA phosphate groups (N/P ratio). The moles of free amine groups in chitosan were obtained from the polymer deacetylation degree (83%). The primary amines of chitosan and the amines of arginine (guanidine group) and histidine (imidazole group protonated at pH 4.5) were used for calculation of the N/P complexation ratio. The moles of phosphate groups were extrapolated from pDNA size (7060 bp), considering that double strand DNA base pairs have 660 g/mol/bp. Amine-phosphate ratio was calculated according to equation 1:

$$ {}^{N}/_{P}\text{ratio} = \frac{\text{moles of amines in the polymer}}{\text{moles of phosphate groups in pDNA}} \quad (1) $$

The nanoparticles were prepared by adding pDNA to the polymer solution at a 1:4 (*v*/*v*) ratio, under vigorous stirring for 2 min. The formed particles were then recovered by centrifugation at 18 000 g for 30 min. For PEI/pDNA, the polyplexes were produced in HEPES buffered glucose (N:P ratio =5; HBG - 20 mM HEPES, 5% glucose, pH=7.1) as recommended in the literature (31).

Nanocarriers Physicochemical Characterization

The hydrodynamic radius and zeta potential of the nanocarriers was determined through dynamic light scattering (DLS) by using a Zetasizer Nano ZS particle analyzer (Malvern Instruments, Worcestershire, UK) Nanocarriers morphology was evaluated by Scanning Electron Microscopy (SEM) as previously described (23). All images were acquired in high vacuum mode and with an accelerating voltage of 20 kV. Image post-processing was performed in Rontec EDWIN software v. 4.1.

Cytotoxicity Assays

The cytotoxicity of CM-PFA polymers and CM-PFA/pDNA nanocarriers was evaluated by the Resazurin assay. In brief, HeLa or hFIB cells were cultured at 37°C, in an incubator with a controlled atmosphere (5% CO_2, 95% O_2, humid atmosphere) until attaining 80 – 85% confluence. The cells were then sub-cultured at an initial density of 8×10^3 cells per well in 96-well culture plates containing DMEM-HG (HeLa) or DMEM-F12 (hFIB) and 10% FBS. After attachment, cells were incubated with different concentrations of CM-PFA polymers (5–200 μg/mL). All experiments were performed at 24, 48 and 72 h. At these predetermined time points Resazurin (1%*w*/*v*) was incubated in each well for a 4 h period, in the dark (37°C, 5% CO_2, 95% O_2). The resultant resorufin pink dye present in culture medium was then transferred to fluorescence plates for immediate analysis (96-well black clear bottom; Greiner Bio-one, Frickenhausen, Germany). Fluorescence measurements were performed in a Spectramax Gemini XS spectrofluorometer (λ_{ex}=560 and λ_{em}=590 nm) (Molecular Devices LLC, USA). Optical micrographs were acquired by using an Olympus CX41 optical microscope attached to an Olympus SP-500 UZ digital camera.

Cell Uptake in Monocultures

Nanocarriers cellular uptake in single HeLa cultures was evaluated by flow cytometry and confocal laser scanning microscopy (CLSM) based on methodologies previously established by our group (23,25). Flow cytometry analysis was performed in a BD FACSCalibur flow cytometer (Becton Dickinson Inc., USA) equipped with green (488 nm) and red (633 nm) lasers. For each experiment a total of 1×10^4 events were collected in the region of interest (ROI) corresponding to HeLa cells. Data acquisition was carried out in the CellQuest™ Pro software. Data processing and statistical analysis was performed in the trial version of FlowJo software v. 10.0.6 (Tree Star, Ashland, Oregon, USA).

For CLSM analysis HeLa cells were innitially cultured at a density of 2×10^4 cells per cm^2, in fibronectin coated μ-slide 8-

well imaging plates (Ibidi GmbH, Germany). After 4 h of nanoparticle incubation the cells were fixed with 4% (*w/v*) paraformaldehyde (PFA) for 10 min at room temperature (RT), permeabilized for 30 min (1% Triton X-100, phosphate buffer saline (PBS)), and stained with the Anti-F-actin CruzFluor® 647 conjugate antibody for 1 h, RT. After rinsing for 6 times with PBS the cells were incubated with Hoechst 33342® for 15 min, RT. Fluorescence images were acquired in a Zeiss LSM 710 confocal microscope (Carl Zeiss SMT Inc., USA). Image processing was carried out in Fiji (32), and Imaris software (Bitplane, Switzerland).

GFP Expression

For transgene expression GFP was used as a model reporter gene. The experiments were performed in 96-well black-clear bottom plates seeded with 1×10^4 HeLa cells per well. Transfection was carried out at a pDNA concentration of 1 μg/cm^2 and by incubating nanoparticles in medium containing FBS and administering to cancer cells during 4 h. After this period the particles were removed. GFP expression was analyzed after 48 h by using a plate reader spectrofluorometer (Molecular Devices, California, USA). In addition, the visualization of GFP expression was carried out by CLSM also after 48 h of transfection.

Targeted Delivery in 2D Co-culture Models

Co-cultures of malignant and normal cells were designed by simultaneously seeding HeLa and hFIB cells in 6-well plates in a 1:2 ratio, using a total number of 2×10^4 cells/well. Co-cultures were maintained in DMEM-HG medium for 24 h prior to all experiments. Targeting specificity was determined in 2D co-cultures by CLSM and flow cytometry. To distinguish normal and cancer cells, HeLa cells were previously transfected with a baculovirus containing an Actin-GFP fusion construct by following the manufacturer's instructions (Backman Cell Light 2.0® Actin-GFP). Co-cultures grown in DMEM-HG / 10% FBS were then incubated with targeted and non-targeted nanocarriers for 4 h. Flow cytometry analysis of co-culture populations was performed in Actin-GFP expressing HeLa cells and unstained fibroblasts. The data of non-treated controls is provided in Supplementary information (Figure S9).

3D Tumor Spheroids Penetration and Gene Expression

Organotypic 3D tumor spheroids of HeLa cells were assembled by using a 3D precision micromold hydrogel scaffold with an array of 81-wells, as previously reported by Napolitano and co-workers (33). In brief, hydrogel micromolds were produced with 2% (*w/v*) liquid agarose by casting a negative scaffold from the original template. After drying, the molds were equilibrated overnight with culture medium. HeLa cells were then seeded to a suitable density and were left to deposit in the various recesses for 4–6 h. MCTS were then grown in the dark (37°C, 5% CO_2, 95% O_2, humid environment), until they reached a mean diameter ranging between 700 and 800 μm. For uptake experiments MCTS were incubated with RITC-pDNA labeled nanoparticles. The spheroids were then rinsed with PBS, fixed (4% PFA, 1 h, RT) and imaged by CLSM. 3D GFP transgene expression was promoted by incubating MCTS with nanoparticles and was then visualized by CLSM after 48 h. All CLSM images were acquired in z-stack mode with an average step of 6.17 μm. 3D reconstruction was performed either in Zeiss Zen software (2010) or Imaris software. The antitumoral effect of the tumor suppressor gene p53 in 3D microtissues was then analyzed. In brief, for p53 gene expression MCTS were transfected with CM-PFA nanocarriers loaded with the pcDNA3-FLAG-p53 expression cassette and spheroids volume was monitored by optical microscopy during 5 days. Measurement of spheroids volume variations were analyzed by image segmentation using automatic image threshold and applying a 2D mask (Fiji software).

Statistical Analysis

One-way analysis of variance (ANOVA), with the post-hoc Newman-Keuls test was used for comparing data of control (negative/positive) and multiple experimental groups. A confidence interval of 95% ($p<0.05$) was considered statistically significant. Data analysis was performed in GraphPad Prism v.6.0 (trial version; GraphPad software Inc, CA, USA).

RESULTS AND DISCUSSION

Synthesis and Formulation of CM-PFA Nanocarriers

The synthesis of folate-targeted multi-amino acid nanocarriers was performed by modifying the native polymeric backbone of low molecular weight chitosan primary amines with various amino acids and also FA-PEG as schematized in Fig. 1a. The successful inclusion of all biofunctional moieties was confirmed by FTIR and ^{1}H NMR spectroscopy (Fig. S1 and S4). The results obtained from ^{1}H NMR spectroscopy reveal that the PEG degree of substitution of chitosan was 46.02 ± 1.38% ($n=3$) (Supplementary information). Also, as demonstrated by Fig. S1 and S2, all the PEG blocks have FA targeting molecules since the characteristic maleimide peak of PEG disappears after thiol-maleimide conjugation between CM-P and FA. These results are corroborated by FTIR data which indicates the presence of the FA characteristic bands as shown in Fig. S4.

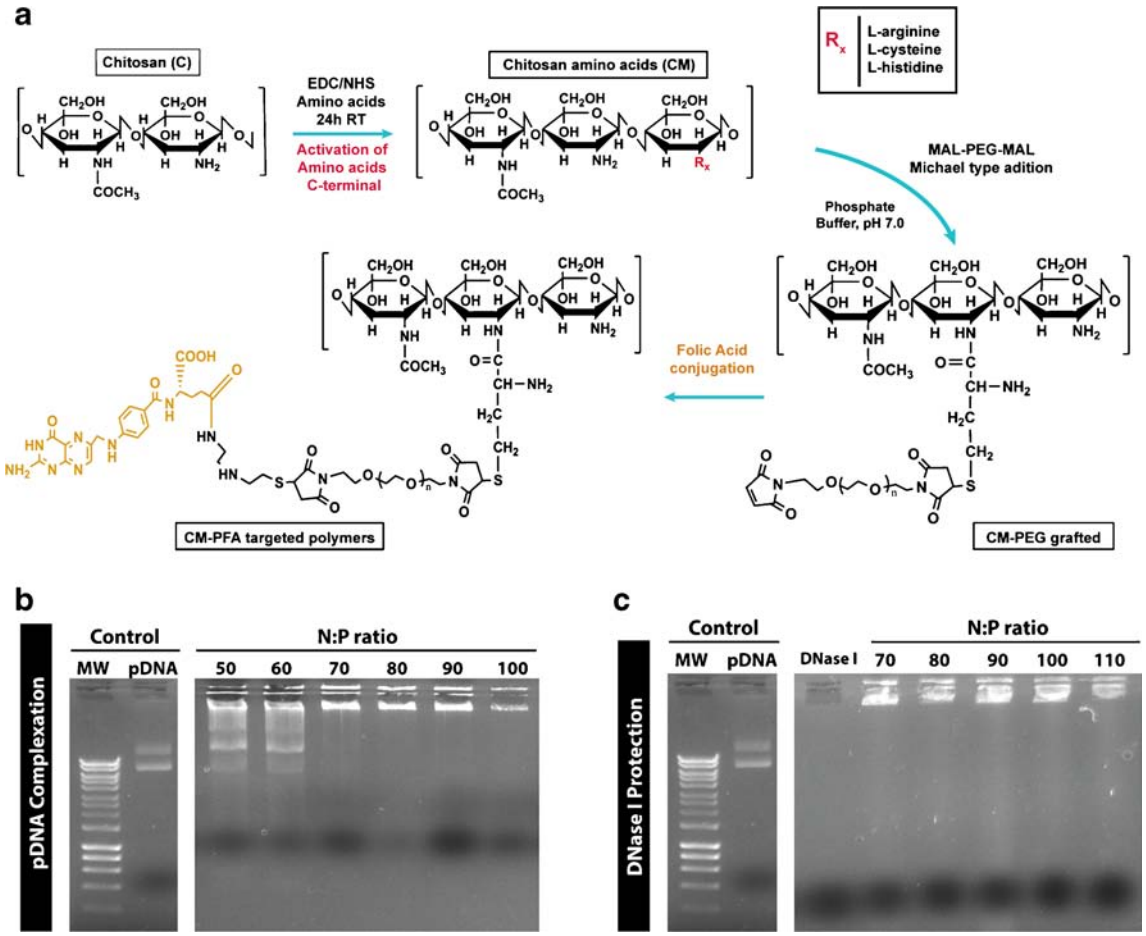

Fig. 1 CM-PFA polymers synthesis and complexation with pDNA. (**a**) Schematics of the chemical functionalization of the native chitosan backbone with amino acids, PEG and FA moieties. (**b**) Agarose gel electrophoresis of CM-PFA/pDNA complexation assay at various amine to phosphate ratios. (**c**) Agarose gel electrophoresis of endonuclease protection assay (DNaseI, 2 U^{-1} , in 5 mM $MgCl_2$, pH 7.4; during 30 min, at 37°C). MW-represents the DNA molecular weight marker. pDNA-represents control naked DNA.

Following CM-PFA synthesis the DNA complexation capacity of the polymer was investigated by agarose gel electrophoresis. The formulation of CM-PFA/pDNA nanocarriers was based on the establishment of attractive electrostatic interactions between polymer amines to pDNA phosphate groups with subsequent self-assembly into nanosized complexes stabilized by grafted PEG chains and decorated with FA. The self-assembled CM-PFA nanoparticles achieve total DNA complexation at a N:P 70 ratio (Fig. 1b). On the other hand, complexes formulated without the FA functionality but with the PEG hydrophilic shell (CM-P) achieve complexation at N:P 40 (Fig. S5). The recovery of the nanocarriers by centrifugation is important to remove free polymer that has not completed with pDNA. The results demonstrate that the CM-PFA complexes formed are highly stable and capable of protecting pDNA from nuclease-mediated destruction as demonstrated in Fig. 1c. This is an important parameter since free DNA is rapidly degraded by serum endonucleases after systemic administration and also in lysosomal compartments (34,35). Therefore protecting DNA biopharmaceuticals is of critical importance since the final therapeutic effect is completely dependent on their structural stability and biological activity (2).

Physicochemical Characterization and Cytotoxicity

The physicochemical characterization of the most stable CM-PFA nanoparticles regarding size, surface charge and morphology is shown in Fig. 2. Overall targeted carriers presented average diameters ranging from 126 nm to 176 nm, with the N:P 90 formulation yielding the smallest particles. The size of non-targeted systems obtained with CM-P polymers was slightly higher than that of the FA-decorated carriers (193 nm to 290 nm) (Fig. S6). The zeta potential of non-targeted carriers was highly positive (+18 to +27 mV), whereas, FA-targeted carriers exhibited slightly negative surface charge, a critical factor for *in vivo* applications (36). From these formulations the CM-PFA N:P 100 particles shown the most negative surface charge (Fig. 2c). The formulations of N:P 70 and N:P 90 demonstrated zeta potentials in the range of

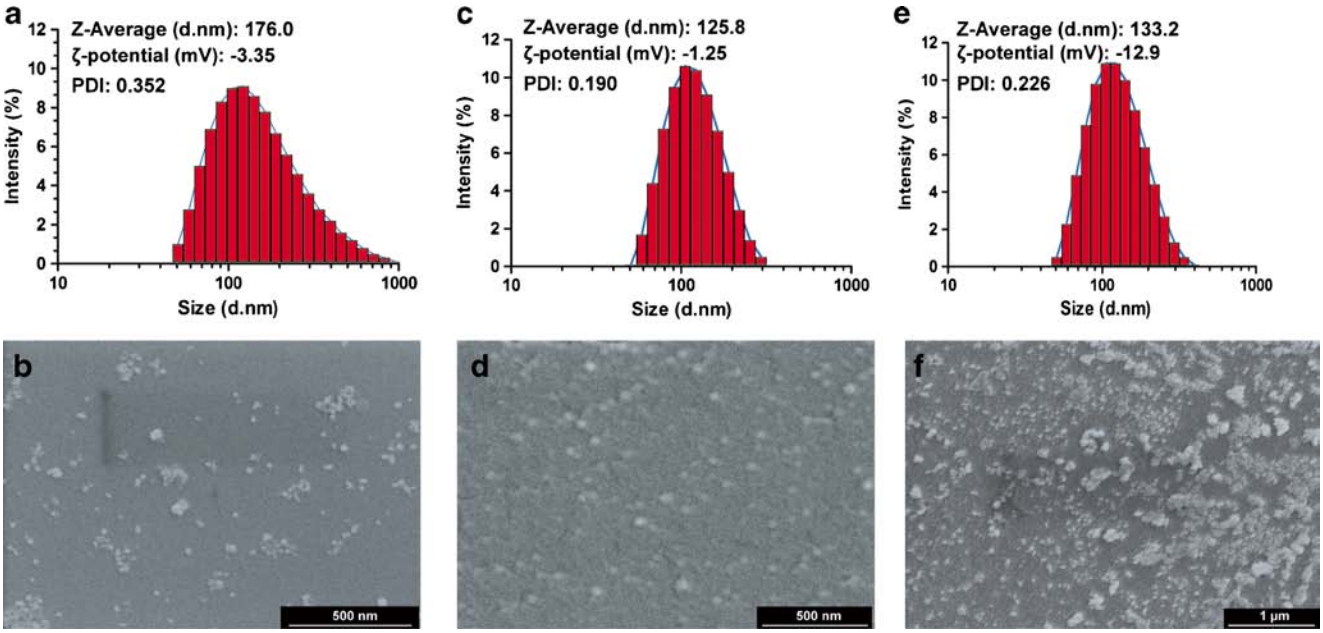

Fig. 2 DLS and morphological characterization of CM-PFA/pDNA nanocarriers. (**a**, **c** and **e**) Size distribution histograms, average size and zeta potential of nanocarriers formulated at N:P 70, 90 and 100, respectively. (**b**, **d** and **f**) SEM micrographs of the morphological characteristics of nanoparticles formulated at the before mentioned ratios.

neutrality (ζ ± 10 mV). From the tested formulations the N:P 70 carriers present the broadest particle size distribution, whereas the N:P 90 nanocarriers exhibited a polydispersity index (PDI) value of 0.19 (Fig. 2c) indicating that the particle size has a narrow distribution (i.e., PDI < 0.2 (37)). These results suggest that this formulation (N:P 90) is particularly suitable for therapeutic applications. The N:P 100 carriers present a PDI slightly higher than 0.2, a value representative of some polydispersity (Fig. 2e). Regarding the morphological characteristics all carriers have displayed spherical-like shapes as revealed by SEM analysis (Fig. 2b, d and f).

To evaluate the potential for intravenous administration the *in vitro* hemocompatibility was studied by quantifying erythrocytes lysis (Fig. 3). The quantitative and qualitative results, indicate a negligible effect on RBCs after incubation with concentrations up to 500 µg/mL (<1% of hemoglobin released). These results are in accordance with the guidelines issued by international agencies (ISO/TR 7406) regarding the critically safe hemolytic ratio, since less than 5% of hemoglobin is released (38). Moreover, as shown in Fig. 3b, SEM analysis reveals that RBCs maintained their characteristic round-shape with a confined central pallor (39), further indicating that CM-PFA based carriers could be administered via intravenous route without deleterious effects for these cells.

In vitro cytotoxicity assays were also performed in both HeLa and hFIB cell lines and have shown that more than 90% viability was obtained at various concentrations and up to 72 h of incubation (Fig. S7). These findings demonstrate the potential of FA-targeted systems for pDNA delivery without eliciting severe toxicity.

Targeted Carriers Cell Uptake and Gene Expression in Single Cultures of Cancer Cells

The effect of FA functionalization of the surface of nanocarriers was expected to increase cellular uptake in folate receptor positive (FR+) cancer cells. Therefore, HeLa cells which over-express the receptors of folic acid according to several reports in the literature (19,40), were selected as target cells for pDNA specific delivery. After cancer cells were treated with equivalent concentrations of either CM-PFA or CM-P nanocarriers for 4 h, the FA functionalized carriers exhibited an evident and significantly higher cellular uptake than non-targeted systems ($p < 0.05$) (Fig. S9 a and b). Among the different formulations of targeted nanoparticles no substantial differences in cellular uptake were observed ($p < 0.05$) (Fig. 4a).

This improved uptake originated a considerably higher GFP transgene expression in cancer cells as shown in Fig. 5a. Actually, in comparison with plain CM-P carriers the targeted particles achieve a noteworthy 3.7 fold increased gene expression (Fig. 5a).

The three different formulations of CM-PFA carriers did not displayed significant differences in gene expression, however since the N:P 90 formulation presents the most suitable conjugation of physicochemical characteristics and biological activity as recently summarized by Ernsting *et al.*, 2013 (36), these carriers were selected for posterior experiments. A visual

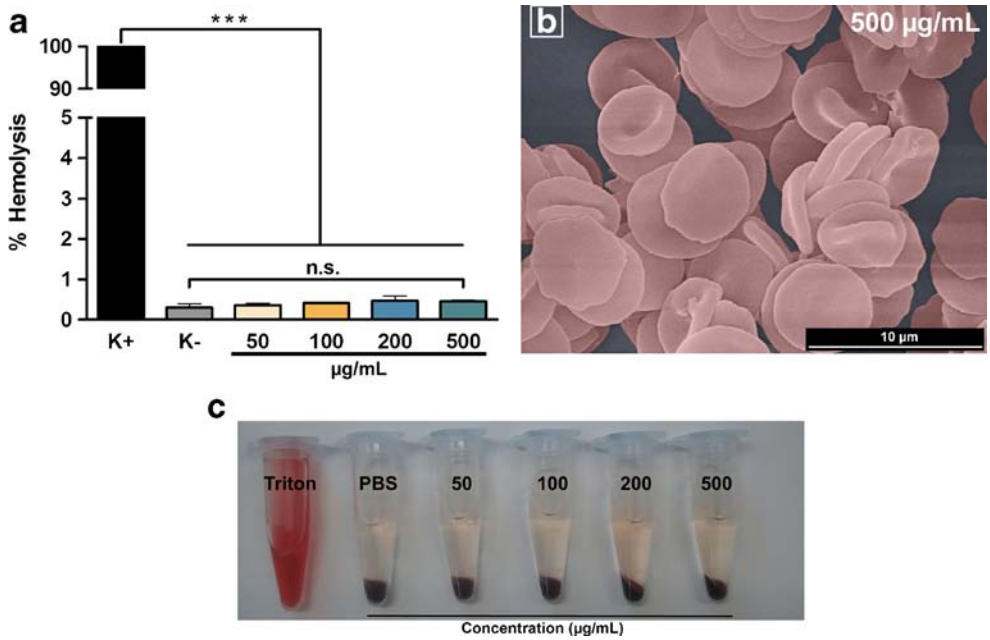

Fig. 3 Hemocompatibility assays of CM-PFA functional polymers. (**a**) UV–vis quantification of RBCs released hemoglobin after incubation with a range of polymer concentrations for 1 h, 37°C. (**b**) Representative pseudo-colored SEM micrograph of RBCs morphology after incubation. (**c**) Optical photograph of the supernatants recovered after the assay for posterior quantification of hemoglobin release. Triton-X 100 was used as positive control for RBCs lysis (K+). PBS was used as negative control. Data is represented as mean ± s.d., $n = 3$; ***$p < 0.001$.

comparison of GFP expression also noticeably reveals the fluorescence intensity differences obtained between PEI 25kDa, non-targeted carriers and FA-decorated systems (Fig. 5b to f). These findings demonstrate the improved delivery and targeting capacity of multifunctional CM-PFA systems in comparison with plain carriers. The relatively low transfection efficiency obtained with PEI is likely due to the transfection conditions used such as the inclusion of serum in the culture medium. This is important since serum presence mimics the *in vivo* conditions. Overall, the fact that gene expression and cellular uptake are simultaneously enhanced supports the hypothesis that including FA-targeting capacity in amino acid-modified nanocarriers further increases their therapeutic efficacy.

To actually confirm that the enhanced cellular uptake and gene expression was directly associated with receptor mediated endocytosis via FR+ cells, a competitive binding assay for the target receptor was performed. For this purpose HeLa cells were incubated with various concentrations of free folic acid and short afterwards with targeted nanocarriers. The obtained results reveal an average 89% decrease in GFP gene expression upon addition of 5 mM of folic acid, and only residual expression is obtained at higher concentration (10 mM) (Fig. S8). Such major reduction supports the concept that CM-PFA carriers are mostly internalized via FR biorecognition.

Targeted Delivery in HeLa:hFIB 2D Co-cultures

2D co-culture models are excellent testing platforms for evaluating the realistic targeting specificity in conditions that closely resemble the actual tumor microenvironment in terms of cell heterogeneity (25). In fact, in comparison with standard *in vitro* cultures, these models offer a more complete approach that takes into account not only the establishment of close cell-cell contacts, but also the cooperative cancer-normal cells response to drugs or genes with anti-tumoral activity (25,41). This combined reaction is commonly associated with the development of an innate resistant phenotype and may affect the therapeutic effectiveness and biological performance of targeted delivery (41). Actually, as recently demonstrated in the seminal work of Straussman *et al.*, 2012, the stromal components of the tumor microenvironment, particularly fibroblasts, assure cancer cells resistance to various anti-tumoral drugs by growth factors secretion (41). This is an important parameter that cannot be evaluated in standard unicellular cultures. Taking this into account, the selectivity of FA-targeted delivery was also evaluated in 2D co-cultures of HeLa and hFIB cells. For these assays, a 1:2 ratio of HeLa:hFIB cells was used as previously recommended in the literature (42). The co-cultured cells remained viable during the course of all experiments and exhibited the characteristic morphologies of both HeLa and hFIB cells as shown in Fig. S7. Fluorescence images revealed that incubation of non-targeted nanocarriers in co-cultures promotes indiscriminate internalization, with CM-P nanoparticles being localized in both HeLa and hFIb cells (Fig. 6a, c, e and g).

On the contrary, upon CM-PFA administration to 2D co-cultures an evident selectivity towards target cancer cells was observed since extensive uptake occurs in HeLa cells and very few fibroblasts have internalized

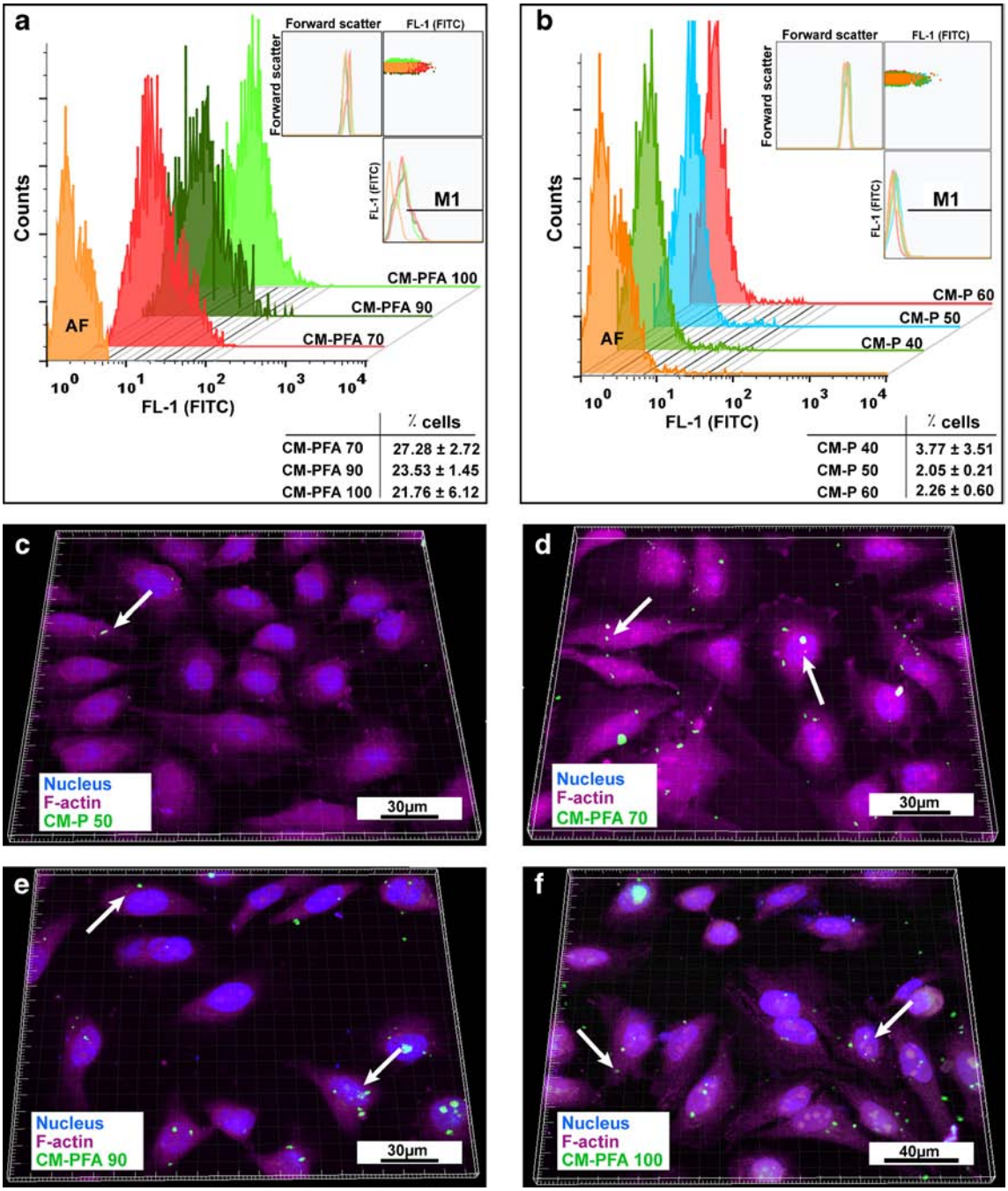

Fig. 4 Flow cytometry and CLSM analysis of nanocarriers uptake in monocultures of HeLa cells. (**a** and **b**) Cellular uptake analysis of targeted CM-PFA and non-targeted CM-P/ FITC-pDNA loaded nanocarriers, respectively. Data represents mean ± s.d., $n = 3$. AF- represents non-treated cells. M1-represents the marker used for analysis of FL-1 positive cells. (**c**) Representative non-targeted nanocarriers cellular uptake.(**d, e** and **f**) Nanoparticle cellular uptake of CM-PFA systems formulated at various ratios. *Blue channel*: Hoechst 33342® labeled nucleus; *Purple channel:* Actin-F-actin Alexa 647 conjugate antibody; *Green Channel*: Pseudocolored CM-PFA/RITC labeled pDNA nanocarriers. *White arrows* indicate nanoparticles.

nanoparticles (Fig. 6b, d, f and h). These results indicate that CM-PFA/pDNA nanocarriers present a genuine affinity for FR+ cells even in the presence of stromal fibroblasts. To further complement these results with a more broad evaluation of targeted nanoparticles uptake in co-cultured cell populations we also studied cell targeting selectivity by flow cytometry in order to obtain a quantitative analysis of CM-PFA particle uptake in cancer cells and normal cells. To distinguish normal cell populations from HeLa cells the latter were stained with an Actin-GFP fusion protein. This approach allowed the separation of both cell types and an individual analysis of

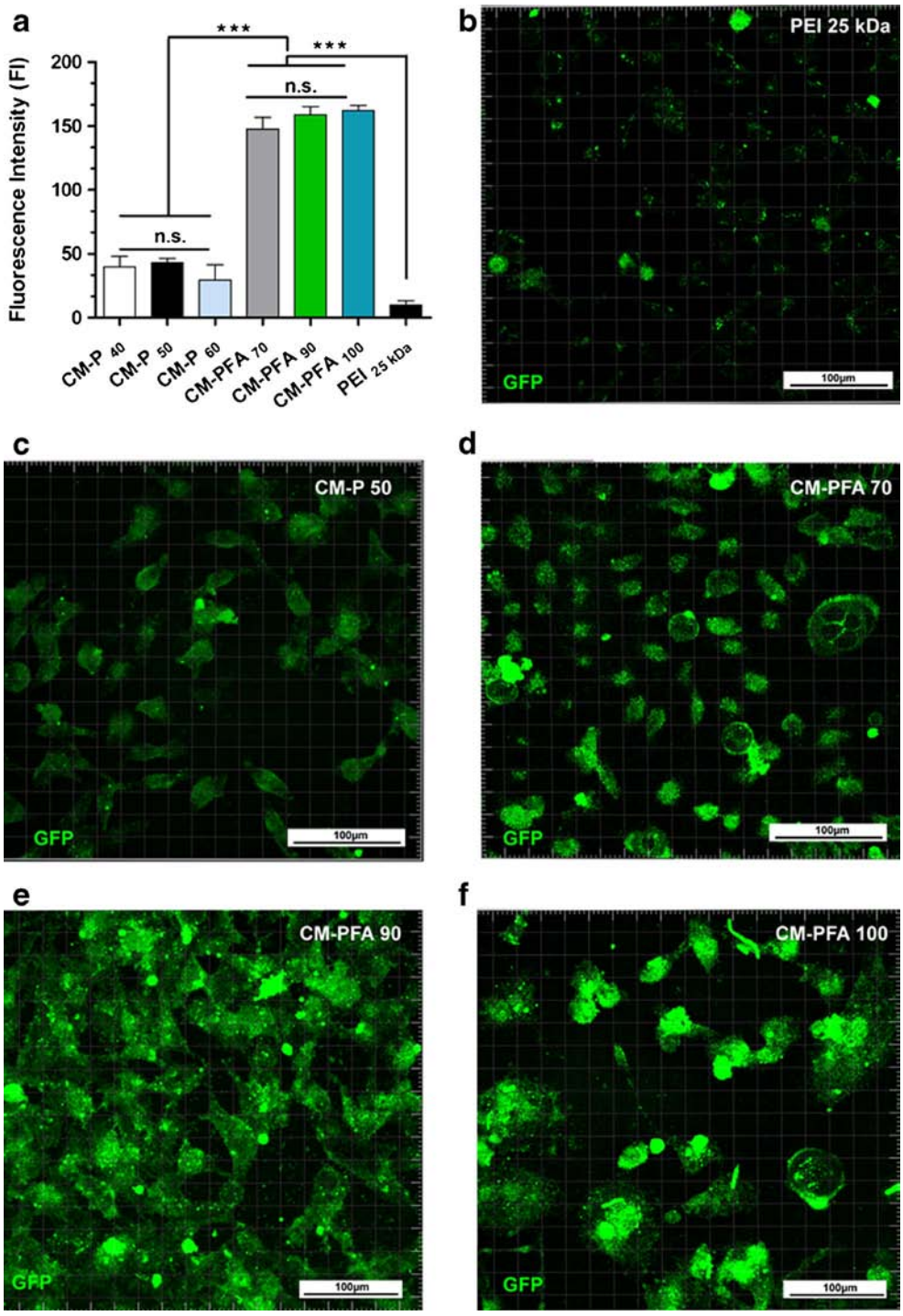

Fig. 5 GFP gene expression in mono-cultured cancer cells. (**a**) Quantification of nanocarriers-mediated GFP expression. PEI 25 kDa N:P 5 carriers were used as controls. (**b** to **f**) Representative fluorescence images of GFP expression. Data is presented as mean ± s.d., $n = 5$, ***$p < 0.001$. n.s.- non significant.

particle internalization. Our findings demonstrated that approximately 30% of HeLa cells have internalized FA-decorated particles, whilst cellular uptake in hFIB cells was negligible (0.84%) (Fig. 7f).

Therefore, when CM-PFA (N:P 90) nanoparticles were administered to a co-culture of FR+ HeLa cells and hFIB (Folate receptor negative) (40), the pDNA cargo is mostly delivered in target cells. Overall, flow cytometry results were consistent with those obtained by fluorescence microscopy. It is essential to underline that these findings were attained in co-cultures that have a higher number of fibroblasts in respect to cancer cells (2:1 ratio). Achieving this degree of selectivity, even in the presence of a higher amount of normal cells, is important to limit off-target events and reduce non-specific cytotoxicity.

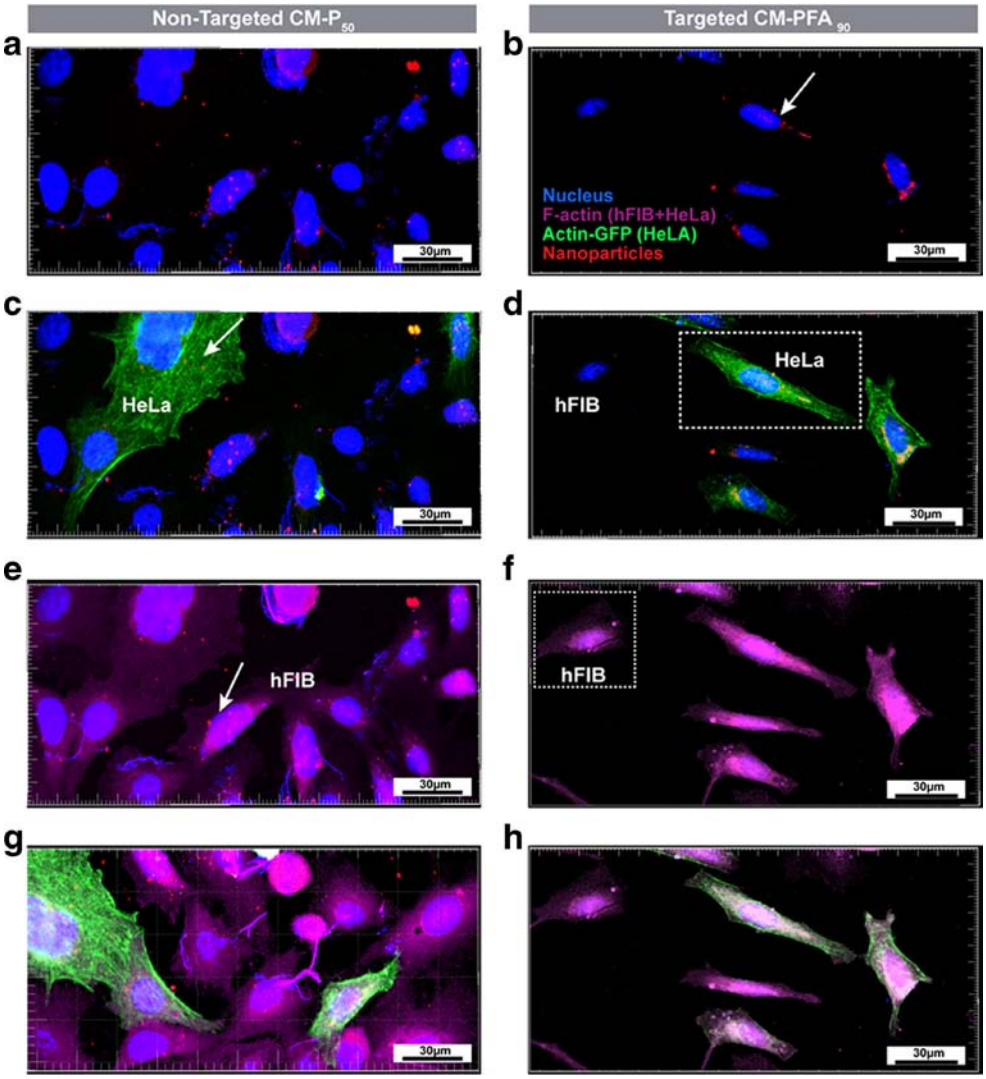

Fig. 6 CLSM analysis of nanocarriers uptake in 2D co-cultures of HeLa and hFIB cells (1:2 ratio). (**a**, **c**, **e** and **g**) Fluorescence images of non-targeted nanoparticles uptake. (**b**, **d f** and **h**) Fluorescence images of FA-targeted CM-PFA/pDNA nanoparticles. *Blue channel*: Hoechst 33342® labeled nucleus; *Purple channel*: Anti-F-actin Alexa 647 conjugate antibody; *Green Channel*: Actin-GFP expressing HeLa cells. *Red channel*: RITC labeled pDNA. *White arrows* indicate nanoparticles.

Nanocarriers Penetration and Anti-tumoral Activity in 3D Microtissues

Self-assembly of HeLa 3D spheroids was carried out in hydrogel micro-molded scaffolds as schematized in Fig. 8a. 3D spheroid models are a unique platform for testing novel nanocarriers since they provide *in vitro* a correlation with *in vivo* solid tumors and are excellent models to study drug or nanoparticle penetration (26). Actually, these 3D models mimic *in vitro* tumors that are poorly vascularized. Penetration into this type of tumors is an issue since generally a poor diffusive transport and limited spatial distribution into deep tumor regions is obtained after drug or nanoparticle administration (43). The assembled 3D spheroid models had sizes in the range of 700–800 µm, an important parameter since it has been described by that spheroids larger than 500 µm possess all the features of solid tumors (e.g. solid structure, necrotic regions, pH and waste gradients) (44). The spheroids also displayed a highly reproducible and defined spherical shape as demonstrated in the optical micrographs of (Fig. 9a to c).

Assuring this high degree of reproducibility is currently only possible due to the use of micromolding-based technologies (33). This manufacturing method presents several improvements in comparison with standard spheroid production techniques and is presently the best high-throughput approach to produce a large number of reproducible microtissues (26). Therefore, the tumor penetration mediated by CM-PFA targeted nanocarriers was evaluated in 3D MCTS in an attempt to investigate nanocarriers therapeutic potential. The CM-PFA targeted nanoparticles achieved considerable penetration in comparison to non-targeted and control PEI25kDa particles (Fig. 8e, f and g). Moreover, a significantly higher number of cells were positive for CM-PFA incubated spheroids as evidenced by the dense and red signal (nanoparticles) observed in Fig. 8d.

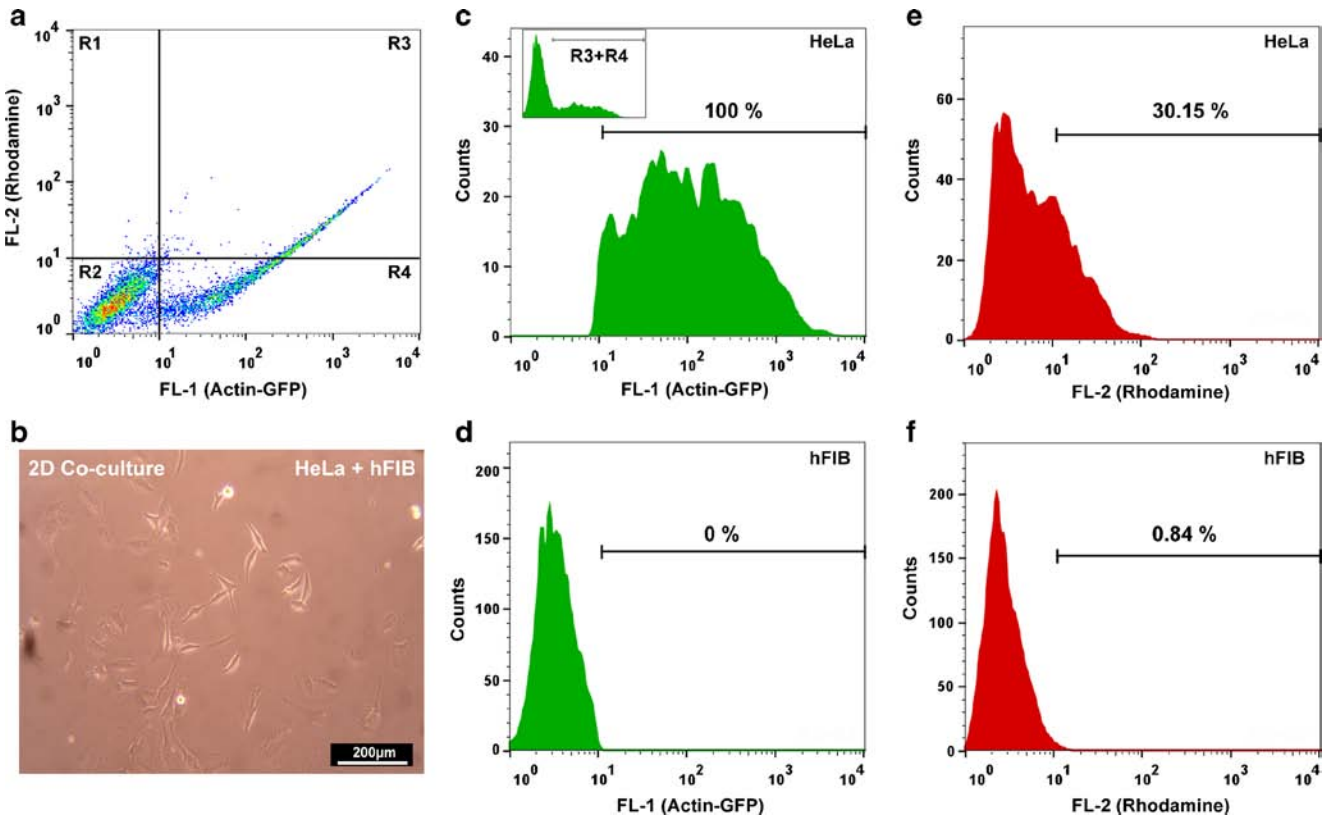

Fig. 7 Flow cytometry analysis of targeting selectivity in 2D co-culture populations. (**a**) Pseudocolor dot-plots of co-cultured HeLa-GFP and hFIB cells. (**b**) Representative optical contrast photograph of 2D co-cultures of HeLa and hFIB cells. (**c** and **d**) Histograms of Actin-GFP fluorescence (FL-1) in HeLa and hFIB cells, respectively. 100% represents the GFP-actin gate used for separating HeLa from hFIB (**e** and **f**) Histograms of CM-PFA/RITC-pDNA nanoparticles (FL-2) in HeLa and hFIB cells, respectively.

We hypothesize that these differences in 3D uptake can be correlated with the effects of FA targeting, but also of zeta potential influence on tumor penetration as recently reviewed by Ernsting *et al.*, 2013 (36). It has been reported that particles with highly positive zeta potential exhibit very limited penetration and distribute non-homogenously inside tumors, whereas particles with zeta potential in the range of (±10 mV) travel further into deep tumor regions and in an homogenous mode (36). Taking into account that control particles (PEI 25kDa) and non-targeted CM-PFA have highly positive surface charge (+25.7 and +18.5 mV, Fig. S4) they are more likely to interact with negatively charged cell glycosaminoglycans (e.g. hyaluronic and sialic acid) and thus showed limited penetration in 3D MCTS. Moreover, as demonstrated in Fig. 2, CM-PFA nanocarriers formulated at N:P 90 present a suitable surface charge for tumor penetration (−1.25 mV). In comparison with nanoparticles functionalized with F3 peptides such as those reported by Hu *et al.*, 2013, the CM-PFA systems achieve approximately 1.86 fold higher tumor penetration, indicating their effectiveness (45). These interesting results obtained in 3D MCTS evidence the necessity of further exploring the effects of targeting and particle surface charge on the extent of tumor penetration in other types of delivery systems. This data can be important in the future to shed light on the most important parameters for improving 3D tissue penetration.

Regarding 3D gene expression, the synthesized CM-PFA systems originated evident GFP expression in MCTS. Actually, has shown by the results of Fig. 9h and the 3D reconstruction (Fig. 9d and g), CM-PFA carriers promoted considerable GFP expression. A quantitative analysis revealed that FA-targeted nanocarriers attained a 8.9 fold higher gene expression in comparison to that of PEI 25kDa nanocarriers and a 7.8 fold higher expression than that of non-targeted CM-P nanoparticles (Fig. 9h, $p<0.001$, $n=10$). To further confirm this therapeutic potential targeted carriers were loaded with a gene expression cassette that encodes the p53 gene with the objective to trigger an anti-tumoral response mediated by this renowned tumor suppressor.

The obtained results after particle administration showed that the administration of CM-PFA/pcDNA3-FLAG-p53 loaded nanocarriers promoted spheroids disruption after 5 days (Fig. 10d to f) in comparison with control spheroids that proliferated during the time of the assay (Fig. 10a to c). A high throughput analysis ($n=25$) based on the automatic segmentation of a large number of treated and non-treated

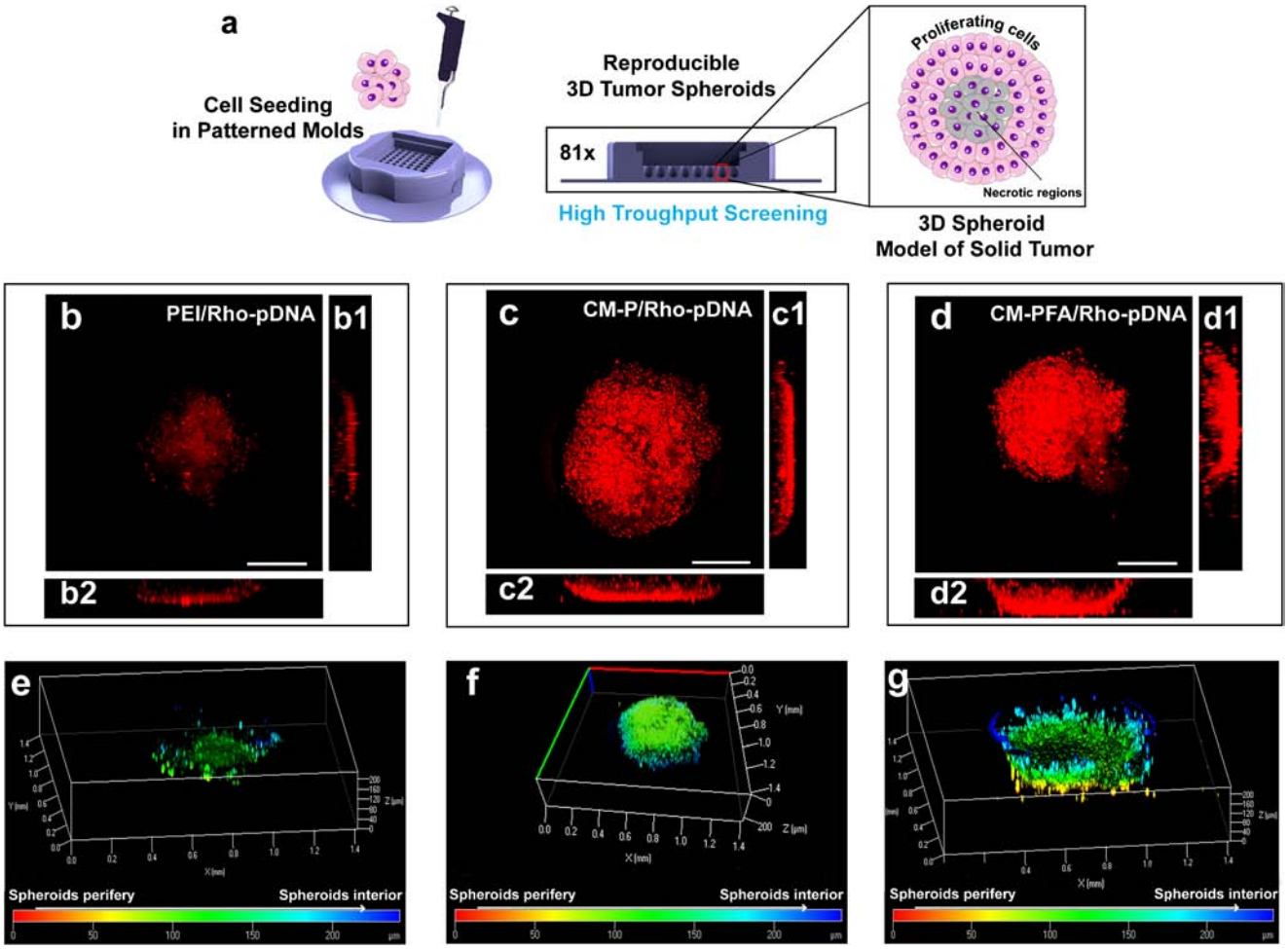

Fig. 8 Analysis of nanoparticle penetration in 3D microtissues. (**a**) Schematics of 3D spheroids manufacture using scaffolds. (**b**, **c** and **d**) Orthogonal projections of PEI 25kDa, CM-P N:P 50, CM-PFA N:P 90 RITC-pDNA loaded nanocarriers penetration in 3D spheroids, respectively. *Red channel*: RITC-pDNA. (**e**, **f** and **g**) Color coded depth analysis of targeted and non-targeted carriers penetration in 3D tumor spheroids. Color bar represents depth in micrometers (μm). PEI 25kDa were used as controls.

spheroids showed that 3D MCTS undergo an average 39% volume reduction after a single p53 administration (Fig. 10g). These findings demonstrate the capacity of CM-PFA systems in terms of both penetration and gene delivery into solid tumor models that closely mimic *in vivo* tumors. These findings emphasize that the novel features of chitosan given by the amino acids modification and folate targeting increase its effectiveness. In fact, in comparison with other chitosan-based drug delivery systems such as those reported by Kim and co-workers (46) this novel chitosan derivative (CM-PFA) presents low cytotoxicity since at 200 μg/mL more than 95% of the cells remain viable (Fig. S7). This is an important characteristic since a higher dose can be delivered without severe side effects. Moreover, the inclusion of amino acids and folic acid in the nanocarriers promotes an enhanced uptake in target cells (Fig. 7) and also an improved lysosomal escape as our group previously demonstrated (23). This improved capacity is associated with the inclusion of both histidine and arginine which promote an escape via the proton sponge effect (23). An effective escape from these vesicles is associated with an improved gene expression. As such, this amino acid modified system presents higher transgene expression in comparison with other folate targeted chitosan nanocarriers such as those described by Shen and co-workers (47). More importantly these systems have evidenced their effectiveness also in 3D tumor models

Fig. 9 GFP expression in 3D tumor microtissues. (**a**, **b** and **c**) Optical ▶ contrast microscopy analysis of 3D tumor spheroids morphology after incubation with control (PEI 25kDa), non-targeted and FA-targeted nanocarriers, respectively. Confocal images of GFP expression in 3D spheroids incubated with targeted (N:P 90) (**d**1 to **d**6)**,** non-targeted (N:P 50) (**d**7 to **d** 12) and control (PEI 25kDa) nanocarriers (**d**13 to **d**18). *Green channel*: GFP expression. *Grey-white channel*: differential interference contrast (DIC) images. The white squares around the 3D spheroids are the recesses of the micro-molded scaffold in which the microtissues are grown. Scale bar represents 700 μm. GFP expression in 3D spheroids mediated by control (PEI 25kDa) (**e**, **e**1 and **e**2), non-targeted (**f**, **f**1 and **f**2) and targeted carriers (**g**, **g**1 and **g**2). (**h**) Analysis of GFP fluorescence intensity in 3D. Data is presented as mean ± s.d., $n = 10$, $^{***}p < 0.001$.

since a significant reduction in the volume of tumor spheroids was obtained (Fig. 10). These results led us to conclude that the CM-PFA system presents suitable characteristics for therapeutic applications.

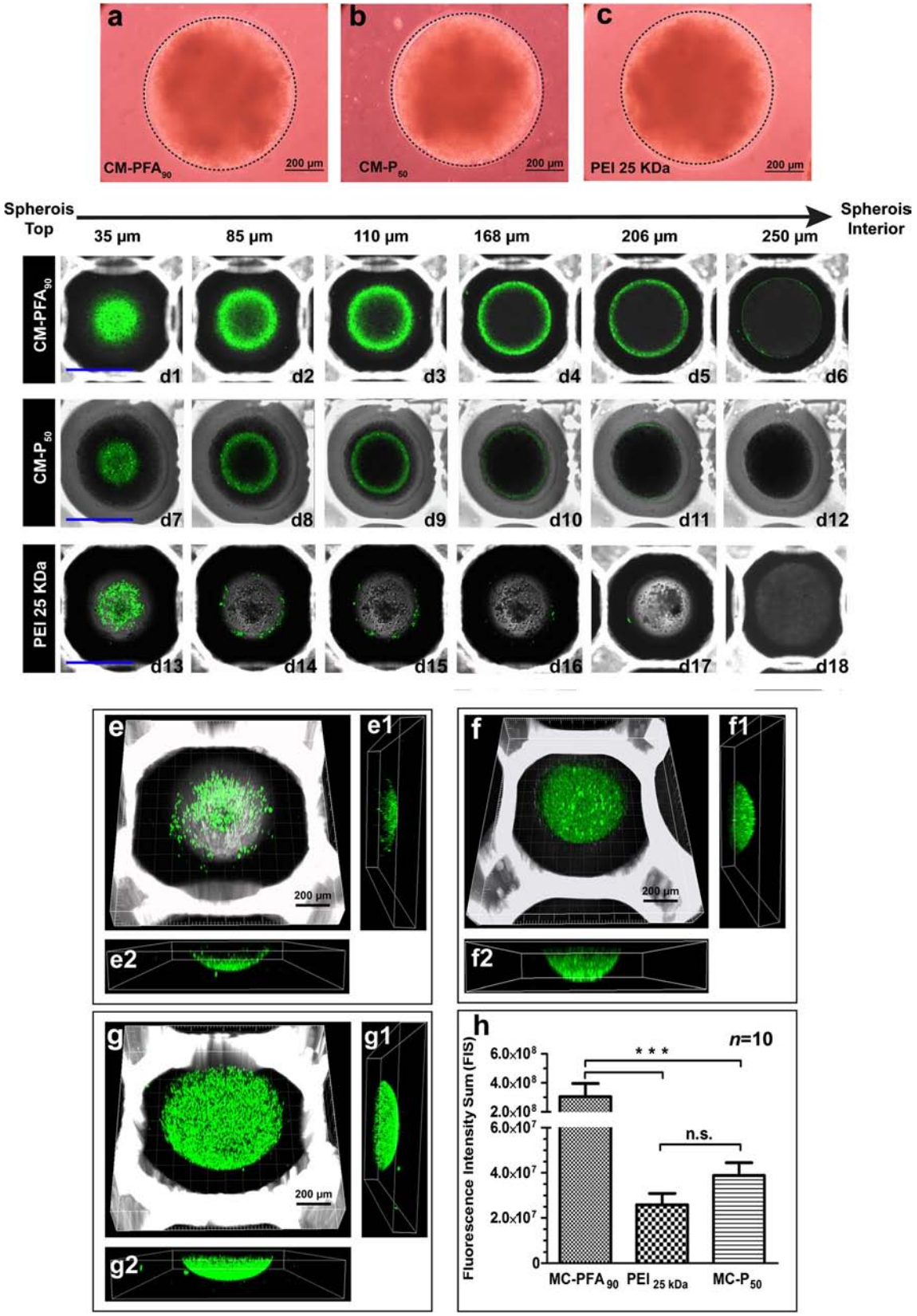

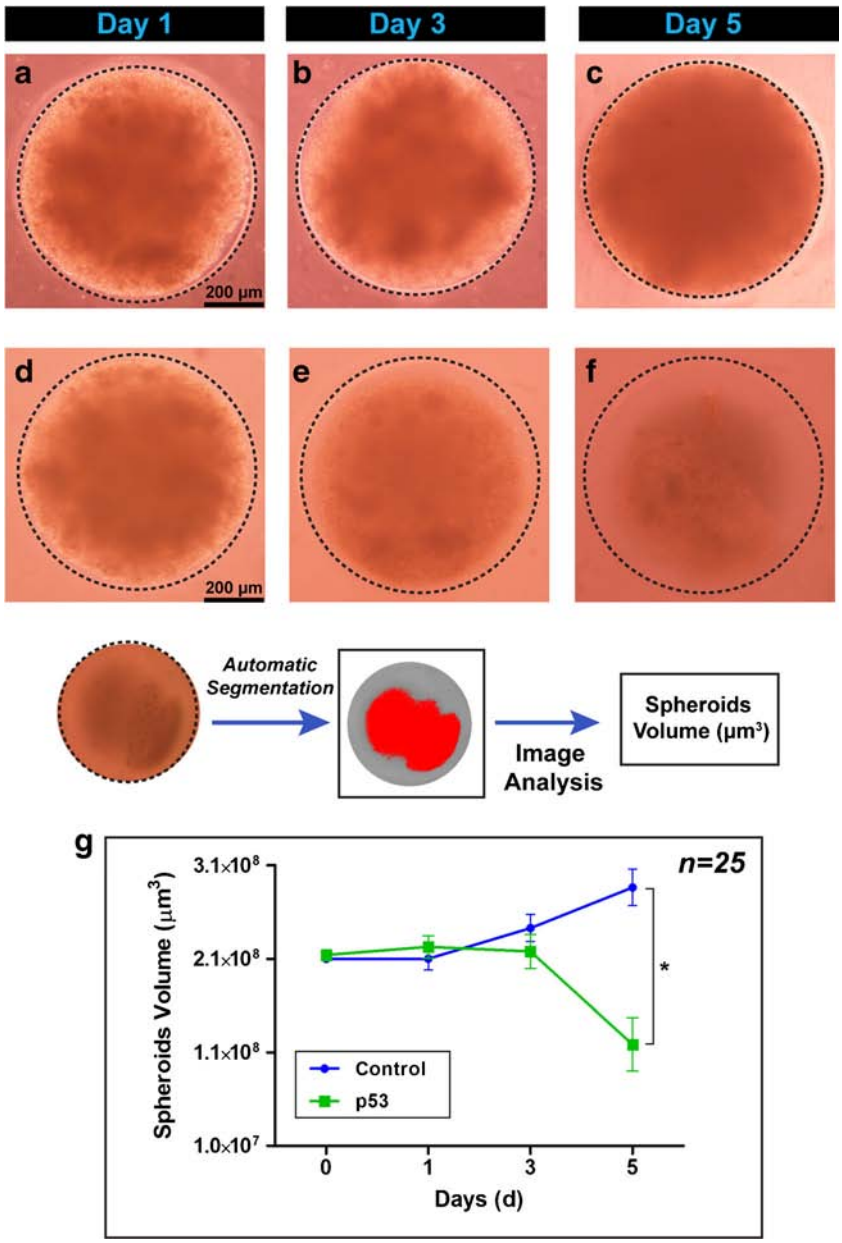

Fig. 10 Evaluation of p53 anti-tumoral activity following CM-PFA delivery of the pcDNA3-FLAG-p53 plasmid to 3D tumor spheroids. Optical contrast microscopy images of non-treated spheroids (**a**, **b** and **c**) and p53 treated spheroids (**d**, **e** and **f**). (**g**) High throughput analysis of spheroids volume reduction after pcDNA3-FLAG-p53 administration during 5 days. Quantification was performed via automatic imaging segmentation. Data is presented as mean ± s.d., $n = 25$, $^*p < 0.05$.

CONCLUSIONS

In this study we synthesized a folate receptor-targeted and PEG grafted amino acid functionalized chitosan-based system for delivery of pDNA biopharmaceuticals into target cancer cells. This novel system assembled in to small nanosized nanoparticles with high hemocompatibility and low cytotoxicity demonstrating proper characteristics for *in vivo* application. The grafted PEG chains further contribute for the stability in physiological conditions and the amino acid moieties have previously shown to enhance exogenous gene expression.

This system exhibited improved cellular uptake and increased GFP expression in monocultures of cancer cells in comparison with non-targeted carriers. Folic acid decoration promoted the establishment of a genuine affinity towards FR+ cancer cells even when closely co-cultured with higher numbers of normal cells. To the best of our knowledge this was the first time that FA-targeted nanocarriers affinity towards target receptors was evaluated in dynamic 2D co-culture models that contained both cancer and stromal fibroblasts. The obtained results provide a rationale for future evaluation of other nanocarriers targeted for different cell receptors.

Moreover, the manufacture of 3D spheroid models with micro-molded templates unlocked the possibility to use testing platforms that provided highly reproducible microtissue models and allowed a high throughput analysis of different experimental conditions. From this standpoint the data gathered in 3D MCTS evidences that these carriers possess

considerable efficiency and also demonstrates that a homogeneous gene expression occurs in 3D. This fact led to an antitumoral effect upon CM-PFA-mediated delivery of the p53 tumor suppressor to 3D MCTS. A part from this, the results obtained with 3D spheroids also indicate that in the future studies concerning the effect of targeting moieties and particle physicochemical properties on tissue penetration should be further characterized. The *in vivo* efficacy and maximum tolerated dose of these nanocarriers will be evaluated in a near future.

Overall, the results led us to conclude that CM-PFA/pDNA nanocarriers present significant potential for future application in cancer therapy.

ACKNOWLEDGMENTS

The authors would like to acknowledge Eng. Ana Paula for her help with the acquisition of SEM images. This work was supported by the Portuguese Foundation for Science and Technology (FCT), (PTDC/EBB-BIO/114320/2009 and PEst-C/SAU/UI0709/2011). Vítor M. Gaspar is grateful for the PhD fellowship from FCT (SFRH/BD/80402/2011). All the authors do not disclose any conflict of interest.

REFERENCES

1. Zhang X-Q, Xu X, Bertrand N, Pridgen E, Swami A, Farokhzad OC. Interactions of nanomaterials and biological systems: implications to personalized nanomedicine. Adv Drug Deliv Rev. 2012;64:1363–84.
2. Gaspar VM, Correia IJ, Sousa Â, Silva F, Paquete CM, Queiroz JA, *et al*. Nanoparticle mediated delivery of pure P53 supercoiled plasmid DNA for gene therapy. J Control Release. 2011;156:212–22.
3. Ragelle H, Vandermeulen G, Préat V. Chitosan-based siRNA delivery systems. J Control Release. 2013;172:207–18.
4. Carocho M, Ferreira ICFR. The role of phenolic compounds in the fight against cancer–a review. Anti-Cancer Agents Med Chem (Formerly Current Medicinal Chemistry-Anti-Cancer Agents). 2013;13(1236–58).
5. Cho H, Lai TC, Kwon GS. Poly (ethylene glycol)-block-poly (ε-caprolactone) micelles for combination drug delivery: evaluation of paclitaxel, Cyclopamine and Gossypol in Intraperitoneal Xenograft Models of Ovarian Cancer. J Control Release. 2013;166:1–9.
6. Maeda H. Tumor-selective delivery of macromolecular drugs via the EPR effect: background and future prospects. Bioconjug Chem. 2010;21:797–802.
7. Bergersand G, Benjamin LE. Tumorigenesis and the angiogenic switch. Nat Rev Cancer. 2003;3:401–10.
8. Decuzzi P, Pasqualini R, Arap W, Ferrari M. Intravascular delivery of particulate systems: does geometry really matter? Pharm Res. 2009;26:235–43.
9. van de Ven AL, Kim P, Haley OH, Fakhoury JR, Adriani G, Schmulen J, *et al*. Rapid tumoritropic accumulation of systemically injected plateloid particles and their biodistribution. J Control Release. 2012;158:148–55.
10. Florence AT. "Targeting" nanoparticles: the constraints of physical laws and physical barriers. J Control Release. 2012;164:115–24.
11. Hollis CP, Weiss HL, Leggas M, Evers BM, Gemeinhart RA, Li T. Biodistribution and bioimaging studies of hybrid paclitaxel nanocrystals: lessons learned of the EPR effect and image-guided drug delivery. J Control Release. 2013;172:12–21.
12. Danhier F, Feron O, Préat V. To exploit the tumor microenvironment: passive and active tumor targeting of nanocarriers for anticancer drug delivery. J Control Release. 2010;148:135–46.
13. Farokhzad OC, Cheng J, Teply BA, Sherifi I, Jon S, Kantoff PW, *et al*. Targeted nanoparticle-aptamer bioconjugates for cancer chemotherapy in vivo. Proc Natl Acad Sci. 2006;103:6315–20.
14. Chen R, Braun GB, Luo X, Sugahara KN, Teesalu T, Ruoslahti E. Application of a proapoptotic peptide to intratumorally spreading cancer therapy. Cancer Res. 2013;73:1352–61.
15. Choe U-J, Rodriguez AR, Lee BS, Knowles SM, Wu AM, Deming TJ, *et al*. Endocytosis and intracellular trafficking properties of transferrin-conjugated block copolypeptide vesicles. Biomacromolecules. 2013;14:1458–64.
16. Panand J, Feng S-S. Targeting and imaging cancer cells by folate-decorated, quantum dots (QDs)-loaded nanoparticles of biodegradable polymers. Biomaterials. 2009;30:1176–83.
17. Chen C, Ke J, Zhou XE, Yi W, Brunzelle JS, Li J, *et al*. Structural basis for molecular recognition of folic acid by folate receptors. Nature. 2013;500:486–9.
18. Mi Y, Liu Y, Feng S-S. Formulation of docetaxel by folic acid-conjugated d-α-tocopheryl polyethylene glycol succinate 2000 (Vitamin E TPGS2k) micelles for targeted and synergistic chemotherapy. Biomaterials. 2011;32:4058–66.
19. Garcia-Bennett A, Nees M, Fadeel B. In search of the holy grail: folate-targeted nanoparticles for cancer therapy. Biochem Pharmacol. 2011;81:976–84.
20. Wu M, Gunning W, Ratnam M. Expression of folate receptor type α in relation to cell type, malignancy, and differentiation in ovary, uterus, and cervix. Cancer Epidemiol Biomark Prev. 1999;8:775–82.
21. C. Aranda, K. Urbiola, A. Méndez Ardoy, J.M. García Fernández, C. Ortiz Mellet, and C.T. de Ilarduya. Targeted gene delivery by new folate–polycationic amphiphilic cyclodextrin–DNA nanocomplexes in vitro and in vivo. European Journal of Pharmaceutics and Biopharmaceutics. 2013;85:390–7.
22. Kogure K, Akita H, Yamada Y, Harashima H. Multifunctional envelope-type nano device (MEND) as a non-viral gene delivery system. Adv Drug Deliv Rev. 2008;60:559–71.
23. Gaspar V, Marques J, Sousa F, Louro R, Queiroz J, Correia I. Biofunctionalized nanoparticles with pH-responsive and cell penetrating blocks for gene delivery. Nanotechnology. 2013;24:275101.
24. HogenEschand H, Nikitin AY. Challenges in pre-clinical testing of anti-cancer drugs in cell culture and in animal models. J Control Release. 2012;164:183–6.
25. Costa EC, Gaspar VM, Marques JG, Coutinho P, Correia IJ. Evaluation of nanoparticle uptake in co-culture cancer models. PLoS One. 2013;8:e70072.
26. Mehta G, Hsiao AY, Ingram M, Luker GD, Takayama S. Opportunities and challenges for use of tumor spheroids as models to test drug delivery and efficacy. J Control Release. 2012;164:192–204.
27. H.-l. Ma, Q. Jiang, S. Han, Y. Wu, J. Cui Tomshine, D. Wang, Y. Gan, G. Zou, and X.-J. Liang. Multicellular tumor spheroids as an in vivo-like tumor model for three-dimensional imaging of chemotherapeutic and nano material cellular penetration. Molecular imaging. 2012;11:487–98.
28. Vargo-Gogolaand T, Rosen JM. Modelling breast cancer: one size does not fit all. Nat Rev Cancer. 2007;7:659–72.
29. Yoshii Y, Waki A, Yoshida K, Kakezuka A, Kobayashi M, Namiki H, *et al*. The use of nanoimprinted scaffolds as 3D culture models to facilitate spontaneous tumor cell migration and well-regulated spheroid formation. Biomaterials. 2011;32:6052–8.

30. Zhang C, Gao S, Jiang W, Lin S, Du F, Li Z, *et al*. Targeted minicircle DNA delivery using folate–poly(ethylene glycol)–polyethylenimine as non-viral carrier. Biomaterials. 2010;31:6075–86.
31. van Gaal EV, van Eijk R, Oosting RS, Kok RJ, Hennink WE, Crommelin DJ, *et al*. How to screen non-viral gene delivery systems in vitro? J Control Release. 2011;154:218–32.
32. Schindelin J, Arganda-Carreras I, Frise E, Kaynig V, Longair M, Pietzsch T, *et al*. Fiji: an open-source platform for biological-image analysis. Nat Methods. 2012;9:676–82.
33. Napolitano AP, Dean DM, Man AJ, Youssef J, Ho DN, Rago AP, *et al*. Scaffold-free three-dimensional cell culture utilizing micromolded nonadhesive hydrogels. Biotechniques. 2007;43:494–500.
34. Fujiwara Y, Kikuchi H, Aizawa S, Furuta A, Hatanaka Y, Konya C, *et al*. Direct uptake and degradation of DNA by lysosomes. Autophagy. 2013;9:1167–71.
35. Chang KL, Higuchi Y, Kawakami S, Yamashita F, Hashida M. Development of lysine-histidine dendron modified chitosan for improving transfection efficiency in HEK293 cells. J Control Release. 2011;156:195–202.
36. Ernsting MJ, Murakami M, Roy A, Li S-D. Factors controlling the pharmacokinetics, biodistribution and intratumoral penetration of nanoparticles. J Control Release. 2013;172:782–94.
37. Johnson RN, Kopecková P, Kopecek J. Synthesis and evaluation of multivalent branched HPMA copolymer − fab' conjugates targeted to the B-cell antigen CD20. Bioconjug Chem. 2008;20:129–37.
38. Maya S, Kumar LG, Sarmento B, Sanoj Rejinold N, Menon D, Nair SV, *et al*. Cetuximab conjugated O-carboxymethyl chitosan nanoparticles for targeting EGFR overexpressing cancer cells. Carbohydr Polym. 2013;93:661–9.
39. Ford J. Red blood cell morphology. Int J Lab Hematol. 2013;35:351–7.
40. Ditto AJ, Shah KN, Robishaw NK, Panzner MJ, Youngs WJ, Yun YH. The Interactions between l-tyrosine based nanoparticles decorated with folic acid and cervical cancer cells under physiological flow. Mol Pharm. 2012;9:3089–98.
41. Straussman R, Morikawa T, Shee K, Barzily-Rokni M, Qian ZR, Du J, *et al*. Tumour micro-environment elicits innate resistance to RAF inhibitors through HGF secretion. Nature. 2012;487:500–4.
42. Delinassiosand J, Kottaridis S. Interactions between human fibroblasts and HeLa cells in vitro. Biol Cell. 1984;50:9–16.
43. Gao Y, Li M, Chen B, Shen Z, Guo P, Wientjes MG, *et al*. Predictive models of diffusive nanoparticle transport in 3-dimensional tumor cell spheroids. AAPS J. 2013;15:816–31.
44. LaBarbera DV, Reid BG, Yoo BH. The multicellular tumor spheroid model for high-throughput cancer drug discovery. Expert Opin Drug Discov. 2012;7:819–30.
45. Hu Q, Gu G, Liu Z, Jiang M, Kang T, Miao D, *et al*. F3 peptide-functionalized PEG-PLA nanoparticles co-administrated with tLyp-1 peptide for anti-glioma drug delivery. Biomaterials. 2012;34:1135–45.
46. Kim Y-K, Minai-Tehrani A, Lee J-H, Cho C-S, Cho M-H, Jiang H-L. Therapeutic efficiency of folated poly (ethylene glycol)-chitosan-graft-polyethylenimine-Pdcd4 complexes in H-ras12V mice with liver cancer. Int J Nanomedicine. 2013;8:1489–98.
47. Shen J-M, Guan X-M, Liu X-Y, Lan J-F, Cheng T, Zhang H-X. Luminescent/magnetic hybrid nanoparticles with folate-conjugated peptide composites for tumor-targeted drug delivery. Bioconjug Chem. 2012;23:1010–21.